Protein Dynamics

International Edition: DOI: 10.1002/anie.201803191
German Edition: DOI: 10.1002/ange.201803191

Nanosecond Dynamics Regulate the MIF-Induced Activity of CD74

Georgios Pantouris, Junming Ho, Dilip Shah, Mansoor Ali Syed, Lin Leng, Vineet Bhandari, Richard Bucala, Victor S. Batista, J. Patrick Loria, and Elias J. Lolis**

Abstract: *Macrophage migration inhibitory factor (MIF) activates CD74, which leads to severe disorders including inflammation, autoimmune diseases and cancer under pathological conditions. Molecular dynamics (MD) simulations up to one microsecond revealed dynamical correlation between a residue located at the opening of one end of the MIF solvent channel, previously thought to be a consequence of homotrimerization, and residues in a distal region responsible for CD74 activation. Experiments verified the allosteric regulatory site and identified a pathway to this site via the MIF β-strands. The reported findings provide fundamental insights on a dynamic mechanism that controls the MIF-induced activation of CD74.*

MIF is a pro-inflammatory cytokine with regulatory functions that control cell fate. In pathological conditions, such as cancer, MIF serves to manipulate the immune system to benefit malignant cells.[1] The cascade of signaling events that promote tumor growth and metastasis is initiated by the MIF-induced activation of the cell surface receptor CD74.[2] MIF is also a non-cognate, partial agonist of CXCR2 and CXCR4.[3] Despite the extensive understanding of the MIF role in immune system physiology and pathology, we still lack a fundamental understanding of all aspects of protein structure and activity. Generation of a co-crystal or NMR structure between MIF and its primary receptor CD74 has been difficult to obtain due to the increased flexibility of CD74.[4] However, insights into the MIF/CD74 interaction can be obtained using other methods that are focused on understanding the intermolecular mechanism of CD74 activation by MIF. Numerous crystal structures of wild-type and mutants of MIF have been determined, as well as MIF co-crystal structures with substrates, competitive, non-competitive, and covalent inhibitors.[5–10] No significant changes in the MIF tertiary or quaternary structures have been observed, other than movements of side chains. Such findings give the impression that local flexibility[11] is important for regulation of MIF biological functions, including activation of the cell surface receptor CD74. The MIF surface residues responsible for activation of CD74 were mapped by epitope scanning[12] and alanine-scanning mutagenesis.[9]

To probe whether local flexibility of the MIF trimer has any role in CD74 activation, we employed atomistic molecular dynamics simulations of wild-type human MIF over 1 μs. Our findings show that the averaged root-mean-square fluctuation (RMSF) over all residues is 0.90 Å indicating that the system remains in a tightly clustered ensemble (Supporting Information, Figure S1a,b). Correlations between fluctuations in the displacement of Cα of pairs of residues i and j were identified with the generalized correlation matrix, with entries C_{ij}. This approach provides an improvement over the calculation of covariance matrices and linear correlations.[13] The approximate threefold symmetry of the protein is reflected in the correlation plot where each boxed region represents a monomer subunit (Figure 1 a). For clarity, we focus on monomer A, and the correlations between residues within monomer A and with residues in monomer A and the other two monomers (B and C). The regions showing strong correlations are highlighted in colored ellipses and circles (Figure 1 a). Within monomer A (red ellipses), the N-terminal residues 1–2 were found to be strongly correlated with three regions: residues 36–39, residues 60–64, and residues 98–99 (Figure 1 b). Similarly, residues 60–64 are also strongly correlated with residues 97–100. The purple circles highlight strong correlations among the residues in monomer A with the other two monomers (Figure 1 a). These residues lie at the three dimeric interfaces and are stabilized by intersubunit β-strand interactions.

In light of these findings, we examined the global network of residues that controls MIF dynamics in fast timescales. As detailed in the Methods section (Supporting Information), we obtained the centrality score from the leading eigenvector of

[*] Dr. G. Pantouris, Prof. E. J. Lolis
Department of Pharmacology, School of Medicine, Yale University
New Haven, CT 06510 (USA)
E-mail: elias.lolis@yale.edu
Dr. J. Ho, Prof. V. S. Batista, Prof. J. P. Loria
Department of Chemistry, Yale University
New Haven, CT 06520 (USA)
E-mail: patrick.loria@yale.edu
Dr. J. Ho
School of Chemistry, University of New South Wales
Sydney, NSW 2052 (Australia)
Dr. D. Shah, Prof. V. Bhandari
Section of Neonatal-Perinatal Medicine, Department of Pediatrics
Drexel University College of Medicine
Philadelphia, PA (USA)
Dr. M. A. Syed, Prof. V. Bhandari
Department of Pediatrics, Yale School of Medicine
New Haven, CT 06510 (USA)
Dr. L. Leng, Prof. R. Bucala
Department of Internal Medicine, Yale School of Medicine
New Haven, CT 06510 (USA)
Prof. R. Bucala, Prof. E. J. Lolis
Yale Cancer Center, Yale School of Medicine
New Haven, CT 06510 (USA)
Prof. J. P. Loria
Department of Molecular Biophysics and Biochemistry
Yale University, New Haven, CT 06520 (USA)
Supporting information and the ORCID identification number(s) for the author(s) of this article can be found under: https://doi.org/10.1002/anie.201803191.

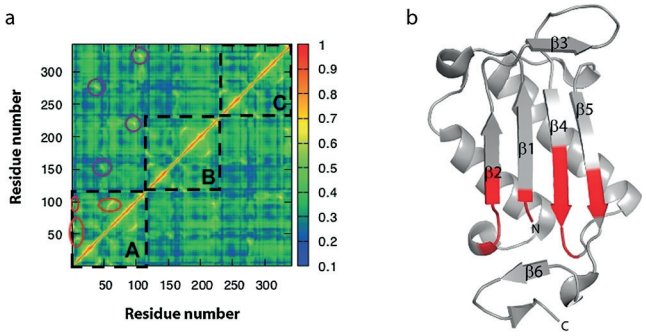

Figure 1. Atomistic molecular dynamics simulations of wild-type MIF. a) Correlation of Cα atoms was derived from a 1 μs simulation using the high resolution structure of wild-type MIF (PDB: 3DJH). Changes in the color, from blue to red, indicate increasing correlation among regions of MIF as shown in the *x* and *y* axes. The three boxes highlight the monomers A, B, and C of trimeric MIF. Correlations within monomer A or between monomer A and monomers B and C are shown in red ellipses and purple circles, respectively. b) The correlated regions within monomer A are illustrated in red.

the generalized correlation matrix (Figure 1 a).[14,15] Residues that are highly connected and/or connected to highly connected residues have a high centrality score and are likely candidates for contributing to global collective motions or signal transmission (Figure 2 a). The residues that demonstrate high centrality scores are marked in red while those with low scores are highlighted in blue (Figure 2 b). Tyr99 is

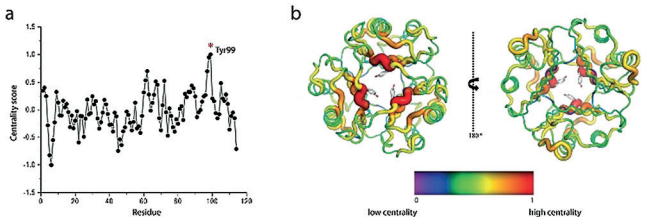

Figure 2. Centrality analysis of the MIF residues over 1 μs simulation. a) Graphical Illustration of the centrality scores of MIF residues over 1 μs simulation. Tyr99, which is labeled with a red asterisk, is the most central residue of all. b) From low to high centrality scores (0–1), the color of each residue reflects its importance associated with the motions of the protein during the MD simulation. Tyr99 is shown as sticks. The two sites of the solvent channel, which is formed by the β-sheets of the three monomers, demonstrate a clear difference with respect to their centrality scores.

the residue with the highest centrality score. This residue is at one end of a solvent channel co-incident with the threefold symmetry of MIF. The high centrality score of Tyr99 was unexpected owing to the absence of any previously assigned role of the solvent channel or Tyr99 in MIF functionality. Noticeably, the two surface exposed sites of the solvent channel exhibit significantly different centrality features (Figure 2 b). From the correlation matrix (Figure 1 a), we find that Tyr99 exhibits highly correlated motions with a number of proximal and distal residues. A graphical illustration of the MIF trimer shows the extent of correlation between Tyr99 and other residues (Figure 3 a). The average

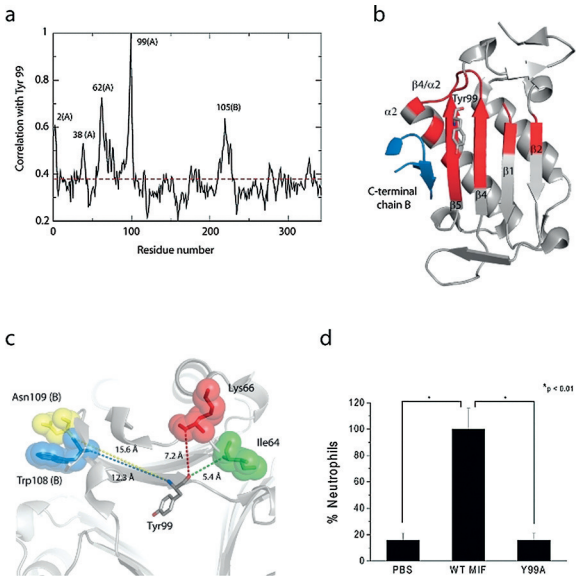

Figure 3. Correlation analysis of Tyr99 and the impact of Y99A mutation on the biological function of MIF. a) Graphical illustration of the regions that are highly correlated with Tyr99. The red dotted line indicates the average correlation. The regions that are correlated with Tyr99 are presented using the residue with the highest correlation value from each region. b) The regions in the MIF monomer correlated with Tyr99 are shown in red. The region correlated to Tyr99 from the adjacent monomer is shown in blue. c) Tyr99 is correlated with distal residues that are located on the surface of MIF and found to have a functional role in activation of CD74. d) Mutation of Tyr99 abolishes the ability of Y99A to activate CD74 in vivo.

correlation is shown as a red dotted line while the regions correlated to Tyr99 are highlighted using the highest correlated residues from various regions. The regions include the catalytic base Pro1, residues located on strands β1 (Met2 and Phe3), β2 (Ala38 and Val39), β4 (Cys59, Ser60, Leu61, His62 and Ser63), the β4/α2 loop (Ile64, Gly65, Lys66, Ile67 and Gly68), the α2 helix (Asn72 and Ser76), residues located near to Tyr99 on the β5 strand (Tyr95, Ile96, Asn97,Tyr98, Asp100, and Met101), and C-terminal residues from the adjacent monomer (Ala103, Ala104, Asn105, Val106, Gly107, Trp108, Asn109, Thr112, and Phe113) (Figure 3 b). Some of these correlated residues (Ile64, Lys66, Trp108, and Asn109) have a functional role in the activation process of the CD74 receptor and are located at distances ranging from 5.4–15.6 Å to Tyr99 (Figure 3 c).[9] We decided to determine whether Tyr99 influenced the MIF-induced activation of CD74.

LPS-free wild-type MIF and the Y99A variant were characterized using an in vivo CD74-dependent lung neutrophil recruitment assay.[9,16] This assay depends on CD74 activation on alveolar macrophages leading to secretion of neutrophil-recruiting chemokines, KC and MIP-2. Although Tyr99 has not been reported to play a role in CD74 activation,[9] the Y99A mutant demonstrates no lung neutrophil recruitment activity in vivo (Figure 3 d). To examine whether lack of activity for Y99A is related to structural instability, we produced ^{15}N wild-type MIF and the Y99A mutant and compared their amide resonances by NMR HSQC experiments. The well-dispersed peaks of Y99A

HSQC spectrum are similar to that of wild-type MIF and show that the mutant is properly folded in solution (Supporting Information, Figure S2a). Resonances in the NMR spectrum of Y99A induced several chemical shift changes in comparison with wild-type MIF (Supporting Information, Figure S2b). The greatest chemical shifts occurred around Lys66, Tyr99 and the C-terminal region and, to a lesser extent, at the N-terminal region. The NMR findings are in agreement with the MD simulations, supporting the predicted correlation between Tyr99 and these regions, albeit at a different timescale (Figure 3a). The X-ray structure of Y99A mutant was determined and has an excellent alignment with the wild-type MIF (RMSD = 0.13 Å; Supporting Information, Table S1, Figure S3a). Comparing the crystal structure of Y99A to wild-type MIF, we also examined how Tyr99 and its mutation affected the solvent channel. We used the software MOLE that analyzes molecular channels and pores to probe potential changes in the size and shape of the MIF solvent channel.[17] Owing to truncation of Tyr99 side's chain, the Y99A mutant significantly increased the size of the channel's opening without affecting either the length or shape of the channel (Supporting Information, Figure S3b,c), supporting that the changes in the crystal structure of the Ala mutation are local. Using MD simulations, we also quantified the number of water molecules in the solvent channels of wild-type MIF and Y99A. Over a 1 μs trajectory, the average number of water molecules in the channel of Y99A increases by 30% (see the Supporting Information), though the specific role of water molecules in MIF activities, if any, remains to be elucidated. We probed the structural role of Tyr99 in the activation of CD74. Using the crystal structure of wild-type MIF (PDB: 3DJH), we explored whether Tyr99 is able to participate in any direct protein-protein interactions. Careful examination of the crystal structure revealed that Tyr99 is located in a groove within the solvent channel with an orientation that does not favor direct interactions with CD74 or any other protein partner (Supporting Information, Figure S4).

To identify a communication pathway between Tyr99 and the distal functional region of MIF involved in CD74 activation, we performed network analysis[18,19] where the edges connecting any two non-neighboring nodes are weighted by the average value of the generalized correlation so that the effective distance for communication between the two nodes shortens when the correlation increases. Using this analysis (see the Supporting Information), we determined the optimal communication pathway between Tyr99 and a receptor-interacting residue, Asn109 in the adjacent monomer, and residues that are likely to be important for allostery. These are Asn97 (from the same monomer with Tyr99), and Val106, Gly107, Trp108, and Ser111 (from the adjacent monomer).[20] Examination of the position of these residues indicates that dynamic signal transmission between Tyr99 and Asn109 occurs via the β-strand system of MIF. To test these predictions, we mutated residues along the communication pathway (N97A, G107A, and S111A), recognizing that the dynamics of the local backbone might be affected by a different side chain (Figure 4a). As a positive control we used the Q24A/Q25A double MIF mutant. These two residues, Gln24/Gln25, are located on the surface of α1-helix, away from the MIF region that is responsible for activation of CD74, and the potential Tyr99 to Asn109 communication pathway. The double mutant is as active as wild-type MIF in neutrophil recruitment in this study as well as in a previous study.[9] Single point mutations of Asn97, Gly107, and Ser111 revealed significantly reduced in vivo neutrophil recruitment activity (Figure 4b). The crystal structures of N97A, G107A, and S111A (Supporting Information, Tables S1, S2) did not reveal any apparent conformational changes that could explain the reduced neutrophil recruitment activity. Superposition of the N97A, G107A, and S111A structures on the crystal structure of wild-type MIF revealed RMSD values between 0.06 and 0.24 Å. From these findings, we conclude that Tyr99 is dynamically associated to the CD74 interacting surface of MIF via signals that travel through the β-strand system of the protein (Figure 4a). The mechanism of signal transmission is consistent with a number of studies of other proteins showing β-strands are able to transmit dynamic signals via backbone hydrogen-bond interactions to distal regions of a protein.[21,22]

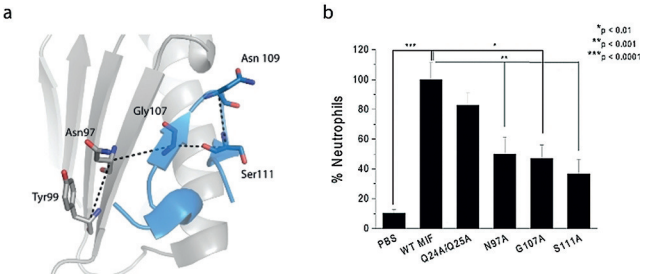

Figure 4. Mechanism of cross-subunit dynamic signal transmission between Tyr99 and the CD74 activation site of MIF. a) Communication pathway between Tyr99 and Asn109, a residue that has a functional role in the activation of CD74 and has a distance of 9.9 Å from Tyr99 of the adjacent subunit. From dynamical network analysis, the communication pathway between the Cα atoms of Tyr99 and Asn109, from the adjacent monomer, is shown as a black dotted line. Tyr99 and Asn97, shown in gray, are always from the same monomer while the remaining residues, shown in blue, are from the adjacent monomer. b) The CD74-depended in vivo neutrophil recruitment assay shows that mutation of the three residues involved in the communication pathway between Tyr99 and Asn109 has a negative impact on the activation of CD74. The Q24A/Q25A double mutant, located on the α1 helix of MIF, was used as a positive control.

In summary, we have found an intramolecular communication pathway by which a residue that is located at the opening of one end of the MIF solvent channel dynamically influences the CD74 activation site of MIF. Communications occur via β-strands. This study provides the foundation for understanding the potential role of dynamics in regulating MIF functions, and identifies a novel allosteric site for drug development.

Acknowledgements

This work was supported by Robert E. Leet and Clara Guthrie Patterson Trust Fellowship Program in Clinical Research, Bank of America, N.A., Trustee (G.P.), the NIH

grants AI065029, AI082295 (E.J.L.) and S10-OD018007-01 (instrumentation grant). Computational and NMR work was supported by the NIH grant GM106121 (J.P.L. and V.S.B.). The high-performance computing resources was supported from NERSC (V.S.B.). J.H. acknowledges support from the Australian Research Council (DE160100807) and supercomputer time from the NCI and Intersect Australian Ltd. The authors thank Dr. Christian Negre (LANL) for sharing his code for performing the centrality analysis.

Conflict of interest

The authors declare no conflict of interest.

Keywords: allosteric sites · long-range communication · MIF · protein dynamics

How to cite: *Angew. Chem. Int. Ed.* **2018**, *57*, 7116–7119
Angew. Chem. **2018**, *130*, 7234–7237

[1] K. D. Simpson, D. J. Templeton, J. V. Cross, *J. Immunol.* **2012**, *189*, 5533–5540.
[2] L. Leng, C. N. Metz, Y. Fang, J. Xu, S. Donnelly, J. Baugh, T. Delohery, Y. Chen, R. A. Mitchell, R. Bucala, *J. Exp. Med.* **2003**, *197*, 1467–1476.
[3] J. Bernhagen, R. Krohn, H. Lue, J. L. Gregory, A. Zernecke, R. R. Koenen, M. Dewor, I. Georgiev, A. Schober, L. Leng, T. Kooistra, G. Fingerle-Rowson, P. Ghezzi, R. Kleemann, S. R. McColl, R. Bucala, M. J. Hickey, C. Weber, *Nat. Med.* **2007**, *13*, 587–596.
[4] A. Jasanoff, G. Wagner, D. C. Wiley, *EMBO J.* **1998**, *17*, 6812–6818.
[5] J. B. Lubetsky, M. Swope, C. Dealwis, P. Blake, E. Lolis, *Biochemistry* **1999**, *38*, 7346–7354.
[6] G. V. Crichlow, C. Fan, C. Keeler, M. Hodsdon, E. J. Lolis, *Biochemistry* **2012**, *51*, 7506–7514.
[7] L. R. McLean, Y. Zhang, H. Li, Y.-M. Choi, Z. Han, R. J. Vaz, Y. Li, *Bioorg. Med. Chem. Lett.* **2010**, *20*, 1821–1824.
[8] Y. Cho, G. V. Crichlow, J. J. Vermeire, L. Leng, X. Du, M. E. Hodsdon, R. Bucala, M. Cappello, M. Gross, F. Gaeta, K. Johnson, E. J. Lolis, *Proc. Natl. Acad. Sci. USA* **2010**, *107*, 11313–11318.
[9] G. Pantouris, M. A. Syed, C. Fan, D. Rajasekaran, T. Y. Cho, E. M. Rosenberg, Jr., R. Bucala, V. Bhandari, E. J. Lolis, *Chem. Biol.* **2015**, *22*, 1197–1205.
[10] E. S. Spencer, E. J. Dale, A. L. Gommans, M. T. Rutledge, C. T. Vo, Y. Nakatani, A. B. Gamble, R. A. Smith, S. M. Wilbanks, M. B. Hampton, J. D. Tyndall, *Eur. J. Med. Chem.* **2015**, *93*, 501–510.
[11] K. Henzler-Wildman, D. Kern, *Nature* **2007**, *450*, 964–972.
[12] D. N. Assis, L. Leng, X. Du, C. K. Zhang, G. Grieb, M. Merk, A. B. Garcia, C. McCrann, J. Chapiro, A. Meinhardt, Y. Mizue, D. J. Nikolic-Paterson, J. Bernhagen, M. M. Kaplan, H. Zhao, J. L. Boyer, R. Bucala, *Hepatology* **2014**, *59*, 580–591.
[13] O. F. Lange, H. Grubmuller, *Proteins Struct. Funct. Bioinf.* **2006**, *62*, 1053–1061.
[14] A. Pandini, A. Fornili, F. Fraternali, J. Kleinjung, *FASEB J.* **2012**, *26*, 868–881.
[15] M. E. Newman, *Phys. Rev. E* **2004**, *70*, 056131.
[16] K. Takahashi, K. Koga, H. M. Linge, Y. Zhang, X. Lin, C. N. Metz, Y. Al-Abed, K. Ojamaa, E. J. Miller, *Respir. Res.* **2009**, *10*, 33.
[17] D. Sehnal, R. Svobodova Varekova, K. Berka, L. Pravda, V. Navratilova, P. Banas, C. M. Ionescu, M. Otyepka, J. Koca, *J. Cheminf.* **2013**, *5*, 39.
[18] M. Girvan, M. E. Newman, *Proc. Natl. Acad. Sci. USA* **2002**, *99*, 7821–7826.
[19] M. E. Newman, M. Girvan, *Phys. Rev. E* **2004**, *69*, 026113.
[20] A. Sethi, J. Eargle, A. A. Black, Z. Luthey-Schulten, *Proc. Natl. Acad. Sci. USA* **2009**, *106*, 6620–6625.
[21] R. B. Fenwick, L. Orellana, S. Esteban-Martin, M. Orozco, X. Salvatella, *Nat. Commun.* **2014**, *5*, 4070.
[22] R. B. Fenwick, S. Esteban-Martín, B. Richter, D. Lee, K. F. A. Walter, D. Milovanovic, S. Becker, N. A. Lakomek, C. Griesinger, X. Salvatella, *J. Am. Chem. Soc.* **2011**, *133*, 10336–10339.

Manuscript received: March 15, 2018
Accepted manuscript online: April 18, 2018
Version of record online: May 9, 2018

